The Astronomical Journal, 139:2159–2169, 2010 June doi:10.1088/0004-6256/139/6/2159

UNUSUAL ^{29,30}Si-RICH SiCs OF MASSIVE STAR ORIGIN FOUND WITHIN GRAPHITES FROM THE MURCHISON METEORITE

T. K. Croat, F. J. Stadermann, and T. J. Bernatowicz
Department of Physics and Laboratory for Space Science, Washington University, Campus Box 1105, One Brookings Drive, St. Louis, MO 63130-4899, USA
Received 2009 July 1; accepted 2010 March 17; published 2010 April 14

ABSTRACT

Correlated transmission electron microscopy and NanoSIMS isotopic studies have revealed two unusual SiCs with large ^{29,30}Si enrichments within micron-sized graphites from the Murchison meteorite. Such anomalies are rare among the overall SiC population (in $\ll$0.01% of SiCs yet measured), whereas two of the three SiCs found within graphite show ^{29,30}Si enrichments, in one case as large as $^{29}Si/^{28}Si = (2.28 \pm 0.03) \times$ solar and $^{30}Si/^{28}Si = (2.03 \pm 0.03) \times$ solar. C-burning and Ne-burning in massive stars ($>8\,M_{\odot}$ initial mass) during their post-main-sequence development are the only processes capable of producing sufficiently large ^{29,30}Si enrichments. This material with heavy Si isotopic enrichments from the O/Ne and O/Si layers is later incorporated into carbonaceous stardust, either in ejecta from Type II supernovae or perhaps in the colliding winds of Wolf–Rayet binaries. Although often too small for Si isotopic measurements, four other SiC-containing graphites show other signatures of a massive star origin. Abundance estimates suggest that such unusual SiCs are present within ~1% of high-density graphites. This abundance can be reconciled with the much lower abundance in the overall SiC population if these unusual SiCs are naturally smaller (~200 nm or less) than SiCs from other isotopic subgroups and if differential destruction of small unusual SiCs occurs in massive star outflows unless these SiCs are encapsulated in graphite.

Key words: dust, extinction – nuclear reactions, nucleosynthesis, abundances – stars: Wolf–Rayet – supernovae: general

Online-only material: color figures

1. INTRODUCTION

Massive stars, including Type II supernovae (SNe), are expected to contribute a significant fraction of the stardust that returns to the interstellar medium, including an estimated ~20% of the carbonaceous dust (Gehrz 1989; Whittet 1992). The large amounts of dust observed at high redshifts (e.g., Bertoldi et al. 2003) must have been formed in a relatively short time after the formation of galaxies, which implies that Type II SNe are the main dust source (Dwek et al. 2007). Various SN models have succeeded in producing the significant amounts of dust (~0.1–1.0 $M_{\odot}$) that would be required to match these observations (Nozawa et al. 2003; Todini & Ferrara 2001). Observations of Type II SNe and supernova remnants (SNRs) do confirm some dust production (e.g., Douvion et al. 2001; Ercolano et al. 2007), although the quantities produced are less than expected (Dwek et al. 2007; Meikle et al. 2007). However, limited information is available as to the nature of this dust, since its spectra are normally broad and relatively featureless. Spectral features do suggest silicates (Arendt et al. 1999) in certain SN layers, and Al_2O_3 and C dust in others, an indication that dust grain formation occurs in a complex and heterogeneous environment. A detailed view of this environment after SN collapse is emerging from studies of optical and X-ray emission lines in SNRs such as Cas A (Rho et al. 2008). Much of the layered structure of the massive star, resulting from the particular nucleosynthetic sequence that occurs during its earlier evolution (Woosley & Weaver 1995), appears to be preserved in the ejecta after its collapse. For example, distinct N-rich, O-rich, and S-rich layers are seen in Cas A (Fesen et al. 2006). However, in other regions of the same SNR, there is evidence of layer mixing and even instances of overturn of layers (wherein Fe-rich matter formed in the interior is later observed outside of the O-rich layers; Hughes et al. 2000; Hwang & Laming 2003). Thus, the environment from which dust grains condense is quite variable in terms of its chemical and isotopic compositions.

In presolar grains from primitive meteorites and interplanetary dust particles (IDPs), we have an inventory of stardust available for isotopic and microstructural study, including carbonaceous phases (SiC and graphite) as well as oxides, silicates, and other refractory grains (Clayton & Nittler 2004). Some of this material clearly originated in SNe or other massive stars, giving unique insights into dust condensation from the complex environments described above. Refractory material with compositions from inner SN zones (e.g., large ^{28}Si excesses presumably from the Si/S zone found in SiC-X grains; Amari et al. 1992) as well as material from outer zones (e.g., ^{18}O enrichments from the He/C zone found in SN graphites; Amari et al. 1995b) have been identified. There are even instances of anomalies from inner and outer SN zones in the same composite grain, such as titanium carbides with decayed ^{44}Ti (from inner Fe/Ni and Si/S zones) found inside SN graphites with ^{18}O excesses (from the outer He/C zone; Amari et al. 1995b). Among the non-carbonaceous grains, there are also some oxides with large ^{18}O enrichments and other isotopic signatures of a massive star origin (Messenger et al. 2005; Nittler et al. 2008).

Oddly though, given the range of anomalies seen from both inner and outer massive star layers, little evidence of anomalies originating from the intervening O-rich layers (e.g., ^{16}O, ^{29}Si, and ^{30}Si enrichments from O/Si, O/Ne, and O/C SN zones; Rauscher et al. 2002) has been found among presolar grains. Until recently, only one unusual SiC had been reported (out of 40,000 + SiCs) with large ^{29}Si and ^{30}Si enrichments characteristic of neutron capture in these regions of massive stars (Amari et al. 1999), although three others have been found recently among smaller size fractions (Hoppe et al. 2010; Zinner et al. 2010). This could be attributable to chemistry, since carbonaceous grains will not form in regions with O > C

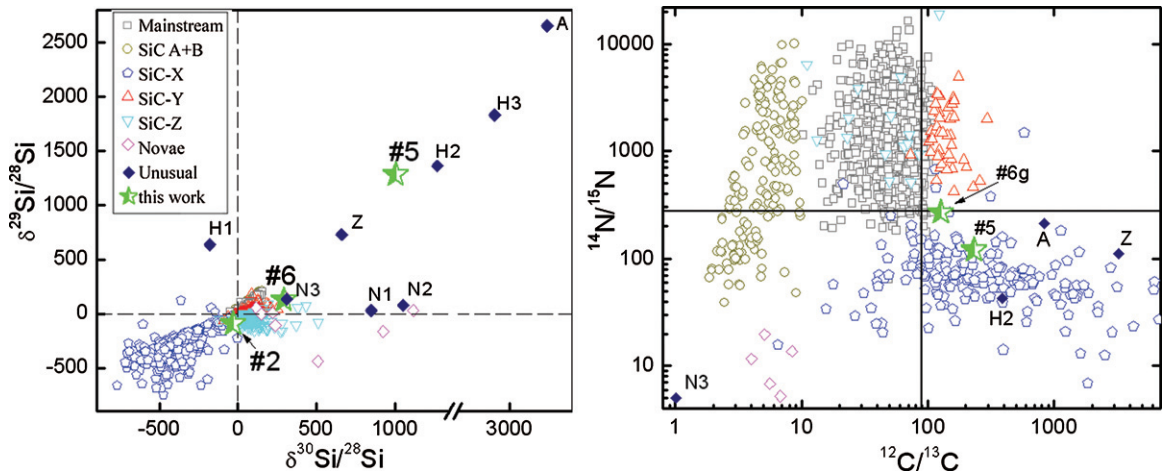

Figure 1. Si isotopic plot of unusual SiC-containing graphites 5 and 6 along with other presolar SiC types (Zinner 2007, and references therein). Plotted ratios are from the SiCs only, with the exception of the N ratio from 6, which is the ratio from the graphite since no N measurement was available from the SiC. No N isotopic measurements are available from unusual SiCs N1, N2, H1, and H3 and SiC 2 from this work. By definition, $\delta^{29}Si/^{28}Si = [(^{29}Si/^{28}Si)_{sample}/(^{29}Si/^{28}Si)_{solar} - 1] \times 1000$. Star symbols are roughly the same size as 1σ error bars.

(A color version of this figure is available in the online journal.)

(Lodders & Fegley 1995), although it may be possible to relax this criterion (Clayton et al. 2001). However, such anomalies also are not common among silicate and oxide presolar grains. Although mild ^{16}O enrichments have been measured among oxides, these are attributed to low-mass red giants (Nittler 1997) and only two oxides with large ^{16}O enrichments (typical of He-, C-, and Ne-burning in O-rich zones of massive stars; Clayton 2003) have been found (Nittler et al. 1998; Gyngard et al. 2010). Further, among the ∼100 silicate grains yet measured (Bose et al. 2008; Nguyen et al. 2007; Vollmer et al. 2008), none have yet been found with the large ^{29}Si and ^{30}Si enrichments expected from neutron capture in the O/Ne and O/C layers (Clayton 2003). Given that ∼40% of the Si from Type II SNe originates in the O/Si, O/Ne, and O/C (calculated from Rauscher et al. 2002 models), it is puzzling to not find more evidence of isotopically heavy Si and other related anomalies among presolar grains. This could be due to differential destruction of such grains in SN outflows (e.g., Jones 2004) or because pressure/temperature profiles are not conducive to dust formation in these zones (Sedlmayr & Patzer 2004). Further, the dearth of such grains could be partly due to limitations of studies done to date, which were not always optimal for detecting such grains. Regardless of the reason for their rarity, when anomalies of this type are found, such presolar grains have increased significance.

Isotopic subgroups are evident in isotopic ratio plots of C, N, and Si of SiC grains (Figures 1(a) and (b)). In many cases, the isotopic subgroups have been traced back to the types of stellar sources that likely produced them (see review by Clayton & Nittler 2004). Mainstream SiCs comprise ∼90% of the population and are inferred to have formed in C-rich asymptotic giant branch (AGB) stars, whereas SiC-Y (∼2% of population) and SiC-Z grains (∼2%) are believed to originate in low-metallicity AGB stars (Amari et al. 2001b; Zinner et al. 2006). SiC-X grains (∼1%) have ^{28}Si enrichments characteristic of the inner zones of SNe (Hoppe et al. 2000). The source of the SiC-A and SiC-B grains (∼5% of population) is still somewhat enigmatic, but these may originate in born-again AGB stars (Amari et al. 2001c). Also a handful of SiCs ($\ll$1%) with low $^{12}C/^{13}C$ and $^{14}N/^{15}N$ ratios have been attributed to novae (Amari et al. 2001a), although more recent results suggest they may be from Type II SN (Nittler & Hoppe 2005). Prior to this study, there were eight unusual grains outside of the isotopic ranges defined above. To determine the abundance of these unusual SiCs relative to entire SiC population, the total number of SiCs measured for Si isotopes must be estimated. Most Si isotopic measurements of SiCs were made in the course of SiC-X grain searches (often isotopic imaging rather than single grain measurements), and in many studies all SiC data were not published (currently only ∼7000 reported Si isotopic measurements of SiCs; Hynes & Gyngard 2009). However, the Si isotopic ratios of over 500 SiC-X grains have been reported and if these in fact comprise ∼1% of the SiC population (Nittler & Alexander 2003), then more than 40,000 presolar SiCs have likely been measured for Si isotopes. Due to the relative abundances of Si isotopes, $^{29,30}Si$ excesses are significantly easier to measure than $^{29,30}Si$ deficits, so any isotopic measurements suitable for SiC-X detection also should have located any unusual $^{29,30}Si$-rich SiCs that were present. Thus, such unusual SiCs comprise ∼0.01% of the overall SiC distribution. Of the unusual SiCs in Figures 1(a) and (b), the two grains with extreme ^{30}Si enrichments and mild ^{29}Si enrichments (labeled N1 and N2 in Figure 1(a); no N isotopic measurement and $^{12}C/^{13}C$ ratios of 150 and 120, respectively) may just be extreme SiC-Z grains with a low-metallicity AGB origin (Nittler & Alexander 2003; Nittler et al. 2006). The third unusual grain (N3 in Figures 1(a) and (b)) shows very low $^{12}C/^{13}C$ and $^{14}N/^{15}N$ (nova-like) but also has high $\delta^{29,30}Si$ and high Al content (Nittler et al. 2006). The fourth (labeled H in Figure 1(a); no N isotopic measurement and $^{12}C/^{13}C$ ratio of 265), believed to be of SN Type II origin, shows a large ^{29}Si excess and a ^{30}Si deficit (Hoppe et al. 2009). The fifth unusual SiC (labeled A with extreme ^{29}Si and ^{30}Si enrichments) clearly has a massive star origin (either Type II SNe or Wolf–Rayet (W-R); Amari et al. 1999). Three more grains of this type have recently been found among smaller size fractions (grain Z from Indarch IH6; Zinner et al. 2010, and grains H2 and H3 from Murchison KJA; Hoppe et al. 2010). Two of these three (grains Z and H2) were also measured for N and, like grain A, showed large ^{15}N enrichments.

Here we report the discovery within a graphite grain of an unusual SiC (labeled SiC 5) with extreme ^{29}Si and ^{30}Si excesses (both $>2\times$ the solar ratios) and ^{12}C excesses, anomalies

that can only be produced in a massive star. A second SiC (6) within graphite (of three yet isotopically measured for Si) was also found with large ^{29}Si and ^{30}Si enrichments, although its origin is slightly ambiguous since it falls into the isotopic range that can conceivably be reached by low-metallicity AGB stars (Zinner et al. 2006). That two of the three SiCs within high-density graphite showed exceptional ^{29}Si, and ^{30}Si enrichment shows that SiCs within graphite have a clearly different isotopic distribution from that of the known SiC distribution, pointing to a unique origin for this type of composite grain. It also suggests that we may find more such unusual SiCs hidden within the existing presolar graphite population using newly developed correlated transmission electron microscopy (TEM) and NanoSIMS.

2. EXPERIMENTAL METHODOLOGY AND SAMPLES

Graphites from the KFC1 density and size separation (2.15–2.20 g cm^{-3}, >1 μm; Amari et al. 1994) of the Murchison meteorite were deposited from suspension, embedded in resin, ultramicrotomed into ~70 nm thick sections, and retrieved on carbon-coated copper TEM grids (further details in Bernatowicz et al. 1996). These graphite slices were then examined with a JEOL 2000FX TEM equipped with a NORAN ultra-thin window energy dispersive X-ray spectrometer (EDXS) and in some cases were examined with a JEOL JEM-2100F TEM. In previous scanning electron microscopy and secondary ion mass spectrometer (SIMS) studies of the KFC1 population (Hoppe et al. 1995; Zinner et al. 1995), ~95% of such graphites have shown C isotopic anomalies, ranging from $2 < {}^{12}C/{}^{13}C < 7300$ (0.02 to 80 times the solar value of 89). Microstructural studies of KFC1 graphites with TEM have revealed different graphite morphologies, including smooth-layered onions (Bernatowicz et al. 1996; Croat et al. 2005) and also more turbostratic "cauliflowers" (Croat et al. 2008). Selected-area diffraction (SAD) patterns and bright and dark field images were used to characterize the structural differences between the graphite types. Since refractory carbides (such as TiC) are commonly found within all presolar graphite types, searches for internal grains were conducted by observation at high magnifications (~10^5) during tilting of the specimen stage, wherein grains as small as 5 nm were revealed at orientations satisfying the Bragg diffraction condition. A total of ~750 unique onion graphites have been observed in TEM studies (Bernatowicz et al. 1996; Croat et al. 2005, 2008), and in some cases multiple ultramicrotome slices were observed from the same graphite. A small subset (~1%) of these onion graphites ($N = 6$) contained internal SiC grains which are the subject of this paper. Since only a single graphite slice was available from most onions, the graphites' original sizes can only be estimated, but generally fall in the 0.8–3.0 μm range. Since the entire graphite's volume was not available for examination and due to an imperfect detection efficiency for small SiCs, the fraction of high-density graphites that contain SiCs could be slightly higher (perhaps as high as ~5% of population). The crystal structures of internal SiCs were determined with SAD and/or microdiffraction, normally on the basis of multiple major zones. In some cases, grains were identified as SiC based on chemical composition and a single unambiguous zone axis (e.g., [0 1 1] zone of 3C-SiC is unique to this polytype). Diffraction rings from {1 0 0} and {1 1 0} graphite served as an internal calibration for d spacings (~1% accuracy).

Although this paper concentrates on SiC-graphites 5 and 6 with unusual isotopic properties, a brief review of currently available data from all six SiC-containing graphites is relevant (see Table 1). The different SiC-containing graphites (all of roughly comparable size) contained 1–26 SiCs with sizes from 15 to 225 nm, with an average abundance of 1.6% by area (maximum of 4.7%) relative to graphite. Three of these SiC-containing graphites (1, 3, and 4) have been investigated with TEM but lack Si isotopic measurements on the internal SiC (Croat & Stadermann 2006; Hynes et al. 2007). Two of these three SiC-containing graphites contain other phases, namely in pure TiCs without *s*-process enrichment in SiC-graphite 4 (Hynes et al. 2007) and Ni-rich kamacite in 1 (Croat & Stadermann 2006, 2008) that are commonly found in low-density SN graphites (Croat et al. 2003) and uncommon or absent from high-density graphites (most of which show evidence of an AGB origin; Croat et al. 2005). The final SiC-containing graphite (3) has an extremely ^{12}C-rich isotopic composition ($^{12}C/^{13}C = 780 \pm 20$), a composition more likely to be achieved in massive stars. AGB stellar models show that ^{12}C enrichments in this extreme can only be reached with initial metallicities of 15%–20% of the solar value and only after the final thermal pulses (e.g., see Tables 1 and 4 from Zinner et al. 2006). Although the strength of evidence varies, the SiC-containing graphites without isotopic evidence of large ^{29,30}Si excesses (e.g., 1–4) have other properties that point toward an origin in massive stars rather than in AGB stars.

Quantitative EDXS analysis was performed on the graphites and their internal carbides. The EDXS background continuum was first fitted and subtracted from the elemental peaks, and peak integrations with 170 eV width (roughly 1.2× the FWHM for Si) were then done centered at the characteristic energies. Sensitivity *k*-factors were derived from geological standards (ilmenite USNM 96189, chromite USNM 117075, basaltic glass USNM 113498) and numerous stoichiometric oxides (lead titanate, lead zirconate, lead molybdate, etc.; see Croat et al. 2005 for further details); spectra were collected with the same operating conditions and analyzed with the same peak integration/background subtraction techniques to increase accuracy. Elemental concentrations were then calculated with a Cliff–Lorimer ratio technique and uncertainties were calculated based on combined errors from both counting statistics (2σ errors) and the *k*-factor error as determined from multiple spectra of standards (typically showing 3%–6% variation). EDXS peak overlaps can introduce additional uncertainties, for example, if low Al signals are sought at the edge of larger Si peaks. To ensure accurate results for Mg and Al concentrations, multiple least-squares fitting with modified Gaussian functions was also done on the Mg, Al, and Si peaks (again after background subtraction), which gave results identical to those from the above method.

After non-destructive analyses were completed, the TEM grid containing these graphites was mounted in a conducting, clamping holder and graphites were analyzed in the Cameca NanoSIMS. A ~100 nm diameter Cs+ primary beam was rastered over the graphites and secondary electrons and negative secondary ions (with various combinations of $^{12}C^-$, $^{13}C^-$, $^{12}C^{14}N^-$, $^{12}C^{15}N^-$ $^{16}O^-$, $^{18}O^-$, $^{28}Si^-$, $^{29}Si^-$, and $^{30}Si^-$) were simultaneously collected in imaging mode. Amorphous Si-rich grains present on the grid were often measured simultaneously using imaging mode and were used as a standard for O and Si isotopic ratios and the carbon film was used similarly as a standard for C. Uncertainties in isotopic ratios were derived from counting statistics (1σ errors) from both the grain of interest and from the nearby isotopically normal regions. Measurement

Table 1
Isotopic Ratios of Both SiC and Graphite (Presented Separately) from Unusual SiC-containing Graphites 5 and 6 as well as Available Data from Other SiC-containing Graphites (all with 1σ errors).

Grain	$^{12}C/^{13}C$	$^{14}N/^{15}N$	$\delta\,^{29}Si$	$\delta\,^{30}Si$	$^{16}O/^{18}O$	SiC Size (nm)[c]	Internal Grains	SiC Composition[d]
SiC 5	233 ± 8	120 ± 9	1280 ± 33	1007 ± 35	550 ± 50	225	1 SiC	$Si_{98.9}Al_{1.0}Mg_{0.1}$
Graphite 5	245 ± 1.5	257 ± 5	206 ± 36	128 ± 40	506 ± 16			
SiC 6	129 ± 5	n/a	128 ± 38	292 ± 48	n/a	105	1 SiC	$Si_{98.9}Al_{0.6}$ (Mg < 0.4)
Graphite 6	126.5 ± 0.7	268 ± 9	62 ± 30	46 ± 34	521 ± 35			
SiCs in 1[a]	99.7 ± 0.4	n/a	n/a	n/a	511 ± 14	35 (13–83)	26 SiCs, 2 kamacites	$Si_{99.2}Al_{0.8}$ (Mg < 0.3)
Graphite 1	110 ± 2	n/a	n/a	n/a	410 ± 33			
SiC 2	13.7 ± 0.2	n/a	−92 ± 56	−30 ± 67	n/a	39 (15–61)	6 SiCs	$Si_{97.3}Al_{1.9}Mg_{0.8}$
Graphite 2	7.6 ± 0.1	n/a	−54 ± 66	−58 ± 78	n/a			
Graphite 3[b]	782 ± 18	n/a	n/a	n/a	577 ± 51	26	1 SiC	Si_1 (Al < 0.4, Mg < 0.3)
Graphite 4[b]	59 ± 1.5	n/a	−16 ± 48	1 ± 57	n/a	35	6 SiCs, 1 TiC	$Si_{99.1}Al_{0.9}$ (Mg < 0.2)
Solar values	89.2	272	0	0	499			

Notes. The SiC sizes and number and types of internal grains found in each graphite are also listed. [a] Aggregated isotopic data from multiple internal SiCs. [b]Independent measurement of internal SiC not possible. [c]Geometrical mean size (average and range presented when multiple grains are present). [d]All reported (SiAlMg)C metals basis compositions in at.%, assuming stoichiometric C; Mg and Al limits in at.% when not detected; best spectrum used when multiple SiCs are present.

time was usually limited by sputtering deterioration and failure of the underlying C support film, and often graphite and SiC were consumed or lost during Si isotopic measurements. Sample motion combined with small signals from internal SiCs (especially those <100 nm) complicated the determination of Si isotopic ratios (which was not possible in a few cases). Further experimental details can be found in Stadermann et al. (2005).

3. ISOTOPIC RESULTS

Based on their Si anomalies, the two unusual SiCs found within graphite and presented in this work (5 and 6) are distinct from the main isotopic subgroups defined by many thousands of previously measured SiCs (Figures 1(a) and (b)). All available isotopic data from the graphites and their internal SiCs are presented separately in Table 1, including any data from SiC-containing graphites 1–4 discussed in Section 2. The most extreme (SiC-graphite 5) exceeds all but three of the unusual SiCs in terms of the combined magnitude of its ^{29}Si and ^{30}Si enrichments, with a large ^{29}Si enrichment that distinguishes it from the extreme SiC-Z grains. Although not as extreme as 5, SiC-graphite 6 is also highly anomalous in Si (10th out of 40,000+ in terms of its combined heavy Si anomaly magnitude). Once one excludes mainstream SiCs with subsolar $^{12}C/^{13}C$, its ^{29}Si enrichment is exceeded only by six unusual grains and a single SiC-Y grain and its ^{30}Si enrichment is also exceeded only by a handful of SiC-Z, nova, and unusual grains (see Figure 1(a)). Whereas SiC 5 lies on an extension of the mainstream correlation line for Si isotopes within errors (defined as $\delta^{29}Si/\delta^{30}Si = 1.3$), SiC 6 (with $\delta^{29}Si/\delta^{30}Si = 0.44$) falls well to the ^{30}Si-rich side of the line, but not as far as many extreme Z and unusual SiCs. The C isotopic ratios of SiC 5 and SiC 6 fall in the range of SiC-X and SiC-Y grains, although 5 is at the upper end of the observed range for SiC-Y grains. Both SiCs within graphite exceed the C isotopic range of all reported SiC-Z grains ($N \sim 120$). SiC 5 shows a larger ^{15}N enrichment than the Amari et al. (1999) grain, but is normal (within errors) in $^{16}O/^{18}O$. SiC 6 was consumed during the simultaneous Si and C measurements, so its N and O isotopic ratios are unknown, although they were measured in the host graphite. For SiC-graphites 5 and 6 and for ∼50 other carbides (mostly TiCs) measured within KFC1 graphites, in each case the C ratios of the internal carbides and their host graphites were similar. However, in SiC-graphite 5, both the Si and N ratios were significantly more anomalous in the SiC than in its host graphite. The $^{14}N/^{15}N$ ratio is 6% lower than the solar ratio in the graphite as opposed to 127% lower than solar in its internal SiC. The Si isotopic anomaly in the graphite is similarly small compared to that of the SiC. Along with the two unusual SiC-containing graphites, a third SiC-containing graphite (called SiC-graphite 2) previously reported by Bernatowicz et al. (1996) has been measured for Si and C. It is isotopically distinct from 5 and 6, with no evidence for ^{29}Si or ^{30}Si enrichments (perhaps even a slight ^{29}Si deficit) and a large ^{13}C enrichment, and as such is most similar to SiC A+B grains. Since it lacks isotopically heavy Si, SiC-graphite 2 is not considered as an unusual SiC in the following discussions, although as will be discussed it does contain evidence for the presence of decayed ^{26}Al.

4. TEM RESULTS FOR UNUSUAL SIC-CONTAINING GRAPHITES

Along with their extremely unusual isotopic compositions, the very existence of these SiCs within graphite is noteworthy. Although refractory carbides such as TiC are common within presolar graphites, SiC is relatively rare (found in only ∼1% of high-density Murchison KFC1 graphites). Microscopic TEM examinations of the unusual SiCs, done prior to destructive NanoSIMS measurements, reveal further detailed information on their properties.

In graphite 5, a ∼290 × ∼180 nm SiC and an adjacent 110 × 110 nm SiC fragment that probably broke off during ultramicrotomy were found at the periphery of the 1.3 μm graphite (Figures 2(a) and (b)). Since no isotopic differences were seen between the two SiC chunks, they are considered as fragments of a single SiC. EDXS measurements of the SiCs show a composition of $(Si_{98.9}Al_{1.0}Mg_{0.1})C$. Tilt investigations over a wide angular range in the TEM ensured that the SiC is an internal grain, rather than being a separate, unrelated grain from the Murchison residue stuck to the surface. These tilting studies also revealed the presence of more than a dozen separate crystalline domains with an average domain size of ∼80 nm (40–105 nm range). Since the domains are significantly smaller than the entire fragments (e.g., 10 domains in the largest fragment), this fine-grained domain structure is not a result of fracture during ultramicrotomy. The sizes of SiC domains in 5 are unusually small in comparison to mainstream

SiCs. Among the hundreds of mostly mainstream Murchison KJB SiCs examined, ∼2/3 consisted of a single crystalline domain (with a mean size of ∼500 nm; Daulton et al. 2003). The SiC domain size in 5 is more similar to those of SiC-X grains (of SN origin), which often have domain sizes near 100 nm but are found as small as ∼10 nm (Hynes et al. 2008; Stroud et al. 2004). Conclusive polytype determinations were made on eight different SiC subgrain domains, seven of which are 3C-SiC normally based on identification of the distinctive [0 1 1] pattern. The other domain was determined to be a 2H/3C intergrowth, based on diffraction patterns obtained separately from the 2H [0 1 −1 1] hexagonal zone and the 3C-SiC [0 1 1] FCC zone. Separate dark-field images showed that the same sample region was diffracting at both orientations, an indication that the 2H domain was below or above the 3C one or possibly formed as a fine-scale intergrowth. By simultaneously rotating virtual models of both polytypes, while keeping their relative orientation fixed, it was found that the (0 0 0 2) 2H hexagonal plane is parallel (within tilting errors) to the (−1 1 1) 3C FCC plane. These planes (e.g., {0 0 0 2} hex and {1 1 1} FCC) are each the most closely packed in their respective polytypes, making this variant of the 2H/3C intergrowth a common one (e.g., Figure 9 in Daulton et al. 2003). It should be noted that some of the seven 3C-SiC domains could conceivably contain undetected 2H intergrowth regions, since only two of the four existing {1 1 1} faces are seen at a given ⟨0 1 1⟩ zone. However, no domains are purely 2H or other higher-order SiC polytypes.

Despite also showing large Si anomalies, the SiC in graphite 6 is microstructurally quite different from that found in graphite 5. This ∼100 nm SiC is located at the center of the graphite (Figure 2(c)), suggesting that the SiC acted as a heterogeneous nucleation site for graphite. EDXS analysis shows a composition of $(Si_{99.4}Al_{0.6})C$ with no detectable Mg. The SiC consists of a single crystalline domain, which was indexed to the 3C-SiC structure based on diffraction patterns from the [1 1 1] and [1 1 0] zones. This 3C-SiC polytype, as well as the 2H/3C intergrowth polytype, are the most commonly found in the overall SiC population (Daulton et al. 2003). However, SiC 6 is unique in that the diffraction is very weak for a grain of this size, suggesting some degree of disorder. Immediately surrounding the central SiC is a thin shell region (∼30 nm wide) that appears lighter in Figure 2(c). Although the thin shell region is too small to measure independently, similar nanocrystalline cores are commonly found inside of ∼2/3 of onion graphites and are surrounded by well-graphitized concentric cages (dark shells in Figure 2(c) that comprise the outer ∼350 nm of the graphite cross section). Diffraction patterns from nanocrystalline cores show {1 0 0} and {1 1 0} rings (from the in-plane graphene sheet spacings) but no {0 0 2} rings from orderly stacking of these graphene sheets in the *c*-direction (Bernatowicz et al. 1996). A disordered central SiC coated by a thin nanocrystalline region and then enveloped in an onion graphite is a peculiar combination of features. These features suggest changing conditions in the condensation environment (as will be discussed below).

TEM studies of SiC-graphite 2 (Bernatowicz et al. 1996) revealed six small SiCs (15–85 nm in size) at the periphery of a ∼0.8 mm graphite (see Figure 1(a) in Hynes et al. 2007). EDXS analysis of the largest SiC shows a composition of $(Si_{97.3}Al_{1.9}Mg_{0.8})C$; Mg/Al = 0.42 ±.06). The Mg content of presolar SiCs is typically very low (0.03 at.% on average from the Amari et al. 1995a study mostly of mainstream SiCs).

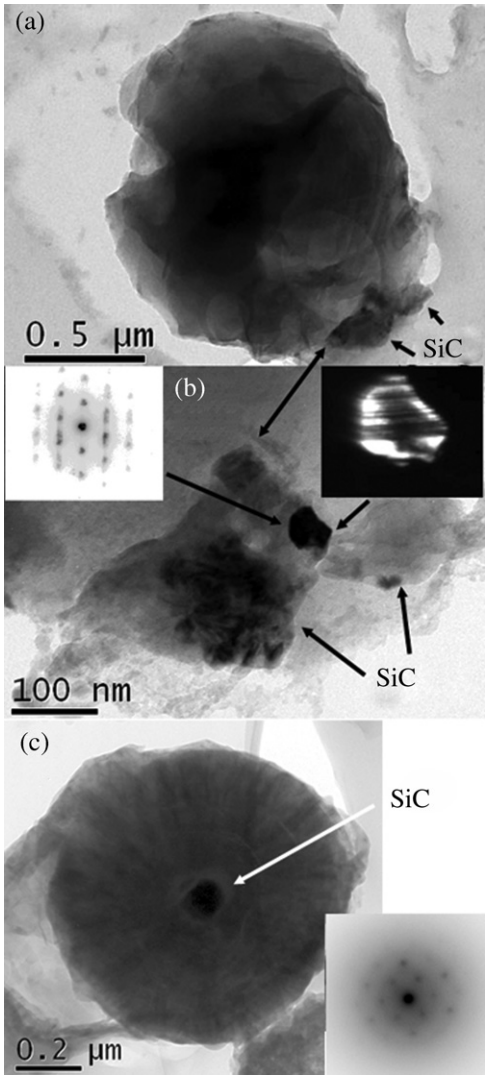

Figure 2. (a) TEM bright-field (BF) image of graphite 5 with internal SiC at periphery. (b) Close-up on SiC grain from graphite 5 showing multiple dark crystalline domains along with inset microdiffraction pattern and dark-field (DF) image shows stacking faults from the darkest SiC domain. (c) BF image of graphite 6 with central disordered SiC (∼100 nm diameter) and inset [0 1 1] FCC diffraction pattern. A thin nanocrystalline shell (∼30 nm thick and lighter in BF image) is visible immediately surrounding the SiC, followed by a transition to well-ordered concentric graphite shells (darker in BF image).

Significant Mg concentrations (up to several at.%) are seen only in SiC-X grains (Hynes et al. 2009). Al–Mg isotopic measurements of such grains have shown that the Mg is often ^{26}Mg from the decay of ^{26}Al, with inferred ^{26}Al/^{27}Al ratios as high as 0.6 (Nittler et al. 1995). Thus, the high Mg content of SiC 2 suggests the presence of decayed ^{26}Al, which is a signature of a massive star. However, this is the only SiC of six measured within different graphites that shows high Mg content.

5. DISCUSSION

Although postulated to originate in the same types of stars (e.g., primarily AGB carbon stars and Type II SNe), presolar graphites and SiCs have quite different C isotopic distributions (Hoppe et al. 1995). Although these differences primarily result from formation in different stellar subtypes (i.e., different metallicities), they could also originate from heterogeneity in

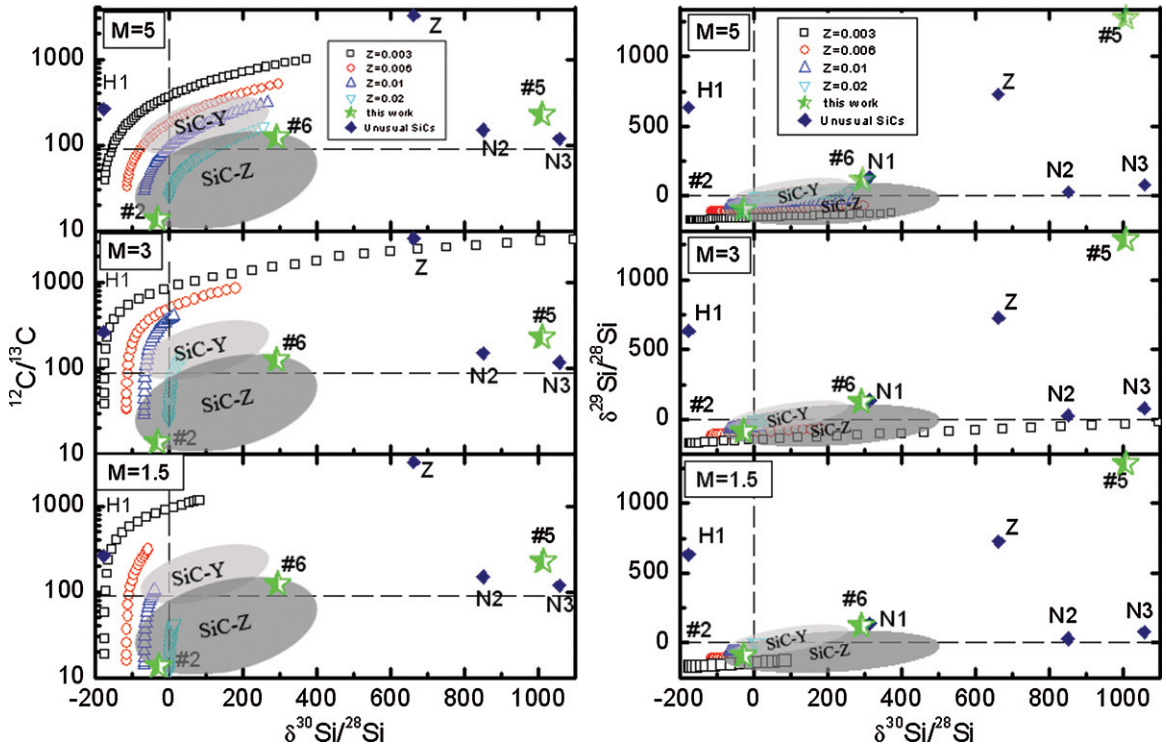

Figure 3. AGB model predictions of C and Si isotopic ratios compared with data from unusual SiCs (those from this study found within graphite along with previously reported unusual SiCs). The AGB model data are reproduced from Zinner et al. (2006) (Torino 1.5, 3, and 5 M_{sol}, Guber cross sections, eta = 0.3 for the 1.5 M_{sol} model, standard ^{13}C pockets; from solar metallicity to 15% of solar). The approximate isotopic ranges of SiC-Y and SiC-Z grains (believed to form in low-metallicity AGB stars) are also plotted. Unusual SiCs labeled A, H2, and H3 in Figure 1, all with $\delta^{30}Si > +1200$ and more extreme than SiC 5, are off-scale to the right in this plot.

(A color version of this figure is available in the online journal.)

outflows from a single star. For this reason, composite grains (SiC in graphite or graphite in SiC; Stroud et al. 2002) are of particular interest in that they constitute a clear case of both phases forming in the same stellar outflow. In this study, not only do we have the isotopic data crucial to making a determination of a massive star origin, but we also have microstructure and morphology determinations from TEM studies from which a phase condensation sequence and any history of processing can be inferred. However, because we currently only have two unusual SiCs in graphite with confirmed heavy Si anomalies and both with a different appearance, the inferences drawn below regarding the astrophysical processes underlying their formation are tentative.

The most stringent constraint on the possible stellar sources of the unusual SiCs in graphite is their extreme Si anomalies, and one must consider as stellar candidates only those that have the capacity to produce carbonaceous dust with large ^{29}Si and ^{30}Si excesses. The major producers of carbonaceous stardust are AGB carbon stars and SNe, with minor contributions from W-R and novae sources (Gehrz 1989). First we consider whether low-mass stars (e.g., AGB stars or novae) could be the source of unusual SiCs. The low $^{12}C/^{13}C$ ratios (<10) universally predicted for novae grains (José et al. 2004) effectively rules out novae as a possible source for unusual SiCs 5 and 6. Zinner et al. (2006) compared the C and Si anomalies predicted by two independent AGB carbon star models (both the Torino/FRANEC and Monash models), including the effects of different stellar masses, initial metallicities, mass loss, and Si cross sections, and the relevant predictions of the Torino model are summarized below. The Monash models give roughly similar projections for C and Si ratios, although these models exhibit hot bottom burning at the larger masses which prevent the formation of carbon stars (Zinner et al. 2006). Figure 3 compares the C and Si isotopic data of the unusual SiCs (from this and previous studies) with model predictions from the Torino models at 1.5, 3, and 5 $M_{\odot}$ (Zinner et al. 2006). For each selected initial mass, the evolution of the C and Si isotopic ratios at four different metallicities (from solar to 15% of solar) are plotted, tracing the star's evolution through successive thermal pulses as it becomes a carbon star (C > O). For the 1.5 $M_{\odot}$ model, the Si anomalies are much smaller than those observed in SiCs 5 and 6, although they do agree with the ratios for SiC 2. As mentioned though, SiC 2 shows indications of ^{26}Al which would not be consistent with a low-mass AGB star. The 3 $M_{\odot}$ model does predict large ^{30}Si enrichments (up to $\delta^{30}Si \sim +1500$ ‰) at the lowest metallicity ($Z = 0.003$), but this model also predicts significantly higher $^{12}C/^{13}C$ and lower $\delta^{29}Si$ anomalies than observed in 5 and 6. Such models come closer to matching the Si isotopic ratios of SiCs with large $\delta^{30}Si$ and more moderate $\delta^{29}Si$ anomalies (e.g., grains N2 and N3), and these may be categorized as extreme SiC-Z grains from low-metallicity AGB stars. The 5 $M_{\odot}$ model after its final thermal pulse does approach the C and Si ratios observed in SiC 6 (especially with solar metallicity, $Z = 0.02$), although SiC 5 and other unusual SiCs (grains Z, A, H2, and H3 in Figure 1; some off-scale in Figure 3) are well outside of this isotopic range. Through process of elimination we are left with only massive stars as the possible stellar sources of these grains. SiC 6 is a borderline case in terms of C and Si isotopes and the diagnostic $^{14}N/^{15}N$ ratio could not be measured. However, its association with other SiCs within graphites that

have unmistakable massive star signatures suggests that it is more likely to be of massive star origin.

Only through neutron-capture reactions in massive stars can the extreme ^{29}Si and ^{30}Si enrichments observed in unusual SiCs be achieved. The most copious dust-producing massive stars are Type II SNe, which are estimated to produce ∼20% of carbonaceous stardust (Gehrz 1989). W-R WC stars are another massive star source of carbonaceous dust, although producing only ∼2% of such dust. Despite their high surface temperatures, carbonaceous dust has been observed around WC stars, either episodically or continuously produced, and this dust formation likely occurs in the colliding winds of WC binaries (Crowther 2007). During their post-main-sequence evolution, massive stars (those with $>8\,M_{\odot}$ initial mass and including Type II SN precursors and WC stars) produce large ^{29}Si and ^{30}Si enrichments in their C-burning and Ne-burning shells, both by neutron capture beginning with ^{28}Si as well as conversion of ^{25,26}Mg by hot alpha particles to ^{29,30}Si (Clayton 2003). Milder ^{29}Si and ^{30}Si enrichments are also present in the He-burning shell, which is exposed on the surface of WC stars.

First we address the possible formation of unusual SiCs in SN ejecta. Due to the stellar structure prior to collapse and subsequent explosive nucleosynthesis, SN ejecta are quite inhomogeneous and condensation of both silicates and carbonaceous dust can occur simultaneously in different zones. The magnitude of heavy Si enrichments in SN ejecta can only be estimated through the use of detailed stellar SN models (although laboratory isotopic measurements of stardust also may provide indirect evidence). Such SN models have commonly been used to explain the isotopic and chemical compositions of SiC-X grains and other SN condensates (Travaglio et al. 1999; Yoshida 2007). To successfully explain SiC-X isotopic ratios, these efforts generally require large-scale mixing of gas from the innermost zones (containing the required large ^{28}Si excesses) with the outer C-rich zones. In contrast, a successful explanation of the anomalies in the unusual SiCs of this study is less convoluted, requiring only mixing between adjacent zones in the intermediate regions of the SN ejecta (neither innermost nor outermost zones). As such, it is surprising that stardust grains with heavy Si anomalies are not more common, either among carbonaceous grains such as SiCs or among silicates. The degree of heavy Si enrichment in the intermediate O-rich zones (O/Ne and O/C) and in the He/C zone can be computed from the 15–25 $M_{\odot}$ models of Rauscher et al. (2002). Here, we define the boundaries of SN zones in terms of mass coordinates using established criteria (e.g., inner O/Ne zone boundary where Ne abundance exceeds Si and outer boundary where C exceeds Ne; Meyer et al. 1995). Then we compute the average isotopic ratios for each SN zone of each model. The result is that the O/Ne and O/C zones have ^{29}Si enrichments of 5–70× solar and ^{30}Si enrichments of 4–170× (both with respect to ^{28}Si) across the 15–25 $M_{\odot}$ mass range. Milder ^{29,30}Si enrichments (1.2–1.7× solar for ^{29}Si and 1.15–2× for ^{30}Si from Rauscher et al. 2002 data) are also predicted for the He/C zone, and this zone also fulfills the other formation requirements (e.g., C/O > 1, ^{12}C/^{13}C > 89) for the unusual SiC-graphites. Thus, anomalies of the observed magnitude can be produced in massive stars.

W-R stars provide another massive star environment in which unusual ^{29,30}Si-enriched SiCs found within graphites could form without requiring an SN explosion. Models of neutron-capture nucleosynthesis in the He-burning cores of these massive stars ($50 < M_{\odot} < 100$) predict isotopic enrichments of 7.2× solar in ^{29}Si and 30× solar in ^{30}Si with respect to ^{28}Si (Amari et al. 1999; Prantzos et al. 1987). Formation of carbonaceous stardust in the winds of W-R stars becomes possible when the stars enter the WC phase, wherein some of the core-He-burning products such as Si appear at the surface (Prantzos et al. 1987). Long-lived structures with 10^4 increased density above those seen in smooth stellar outflows, in which dust can form, are observed in W-R outflows (Williams 2008), and are likely exclusive to the binary systems that constitute more than half of the observed W-R stars (Crowther 2007). Infrared spectral energy distributions of such regions are consistent with amorphous carbon formation, although SiC has not been detected (Cherchneff et al. 2000). Without the turbulent mixing of an SN, the ability of the overproduced ^{29,30}Si to escape into the WC winds is more limited, resulting in lower but still considerable ^{29,30}Si isotopic enrichments (<5× solar; Prantzos et al. 1987). These winds are also predicted to have very high ^{12}C/^{13}C ratios that exceed those seen in the unusual SiCs. However, mixing of the WC star outflows with the stellar envelope of the binary companion provides a natural mechanism for dilution of excess ^{12}C (Amari et al. 1999), and thus can provide another plausible route to the formation of ^{29,30}Si-enriched unusual SiCs.

Like the SiC-X grains of SN origin and unlike mainstream SiCs, the unusual SiC found in SiC-graphite 5 is comprised of small crystalline domains. Comparative studies of mainstream and SiC-X grains from the same Murchison size fraction (KJG; ∼3 μm diameter) show considerably smaller crystalline domains among the SiC-X grains, which suggests more rapid nucleation and growth of both SiC-X grains (Hynes et al. 2009) and by analogy the unusual SiC 5. However, most SiCs within graphite (including 5) differ from SiC-X in that they do not show high Mg/Al ratios (with median Mg/Al ratio ∼0.6) indicative of ^{26}Mg from decayed ^{26}Al, a feature only seen in SiC-graphite 2. The SiC in 5 lies at the periphery of the graphite (Figure 2(a)), and thus clearly did not act as a heterogeneous nucleation site for the graphite, but more likely indicates SiC formation independent of graphite, either contemporaneously or after graphite formation. This differs from the TiC-containing high-density graphites, which along with being ∼15× more common than SiC-containing graphites, are usually found with a TiC at the graphite's center (Croat et al. 2005). With only a single ultramicrotome slice of SiC-graphite 5, we have insufficient material to know whether or not TiCs were also present in this graphite or whether one may have served as its nucleation center. To address this question, serial ultramicrotomy of entire high-density graphites that contain large ^{29,30}Si and ^{12}C enrichments are planned. Observations of SiC-graphite 5 suggest the most likely sequence of phase condensation is graphite and then SiC. Except for the lack of internal TiCs, this is consistent with predicted phase condensation sequences from detailed thermodynamical equilibrium calculations of condensation from a C-rich gas (albeit for AGB outflows and not massive stars: Lodders & Fegley 1995; Sharp & Wasserburg 1995). Thermochemical modeling efforts have also been extended to grain condensation in Type II SN ejecta (Fedkin et al. 2009; Lodders 2006). Despite the complex non-equilibrium processes occurring in massive stars (e.g., reverse shocks in Type II SNe or colliding winds in binary W-R stars), previous observations of SN graphites are roughly consistent with the predicted phase condensation sequences, as these graphites almost always contain numerous refractory TiCs but rarely contain the less-refractory SiC phase. Thus, the absence of TiCs within graphite 5 is somewhat unexpected, and may reflect significant deviations from a gas of solar composition.

Some outer SN regions have a pressure, temperature, and composition conducive to the formation of SiC-graphites similar to 5. The necessity of C/O > 0.98 for graphite formation (Lodders & Fegley 1995) restricts consideration to the He/C zone and the bottom of the He/N zone. In these regions, graphite is predicted as the first condensate (at $T > 2000$ K) and SiC is also a high-temperature condensate (Fedkin et al. 2009). Thus, SiC-graphites similar to 5, with the SiC found at the periphery of the graphite, could reasonably condense in such an environment. However, the magnitude of the Si anomalies in the C-rich regions (He/C and He/N SN zones) is not sufficient to produce the large ^{29,30}Si enrichments seen, so some material from adjacent O-rich regions (e.g., O/Si, O/Ne, O/C SN zones) with larger heavy Si enrichments is required. An admixture of ∼2% of the material from O-rich zones can roughly reproduce the observed isotopic ratios while still adhering to the C/O > 0.98 criterion, although the persistent problem of obtaining the correct ^{29}Si/^{30}Si ratio remains (Travaglio et al. 1999). The particular mixtures of SN ejecta that can reproduce the isotopic anomalies found in unusual SiCs have lower Si abundance (e.g., Si/C ratios ∼5× lower) than the mixtures required to reproduce the SiC-X grain isotopic anomalies. Thus, the fact that the overall sizes of unusual SiCs in graphite are considerably smaller (∼10×) than typical SiC-X grains is consistent with the expected lower Si abundance.

The typical predicted condensation sequences above make SiC 6 more exceptional, wherein a disordered central SiC has apparently acted as a nucleation site for graphite. The concentric shell structure of onion graphites allow us to very accurately determine the position of their centers, and the probability of a grain appearing at the center by chance is calculated at ∼1% (e.g., Bernatowicz et al. 1996). Further supporting evidence of the idea that carbides do act as graphite nucleation centers comes from studies of other onion-like graphites (Bernatowicz et al. 1996; Croat et al. 2005). When a TiC was found among single ultramicrotomed sections of well-graphitized high-density onions, in over 60% of cases (20 of 33 graphites; Croat et al. 2005) the TiC was directly at the center of the slice. If the TiCs formed later and were randomly occluded into graphites during their growth, the fraction of onion graphite spherules with carbides directly at their centers would have been at least ∼10× lower. The graphitic material that first condensed around SiC 6 is a thin nanocrystalline region. Such nanocrystalline regions were previously shown to consist of clusters of graphene sheets with <1 nm diameter that are aggregated without orderly stacking in the *c*-direction (Bernatowicz et al. 1996). Then graphite condensation proceeds via growth of the more-ordered concentric rims that form the exterior of onion graphites. Bernatowicz et al. (1996) argue that the nanocrystalline cores result from carbon condensing rapidly at high supersaturation, followed by a transition to lower partial pressures and thus slower growth of the more-ordered rim regions.

The observed condensation sequence of SiC than graphite in SiC 6, when considered along with predicted condensation sequences in AGB stars and observations of other AGB graphites, argues against an AGB origin for this grain. Equilibrium thermodynamical calculations, which are often consistent with the condensation sequences inferred from observed grain assemblages, generally do not predict SiC formation before graphite in AGB star outflows and this is especially true for lower metallicities (due to lower Si partial pressures). The order in which TiC, SiC, and graphite condense in carbonaceous grain assemblages is a function of C/O ratio and pressure (Lodders & Fegley 1995). Lodders & Fegley (1995) considered a range of pressures and C/O ratios (with otherwise solar abundances) and found that the SiC condensation temperature only exceeds that of graphite at relatively high total pressures (10^{-2} to 10^{-4} bars) and with C/O ratios near unity. Additionally, TiC is always predicted to condense before SiC (and none are found in graphite 6), although due to lower Ti abundance there are stronger kinetic limitations for TiC growth than for SiC. Based on kinetic considerations and astrophysical models, Sharp & Wasserburg (1995) estimate the pressure range for carbonaceous grain growth in AGB environments to be $0.2 < P < 40$ dynes cm^{-2}. They similarly conclude that SiC will form before graphite only at low C/O ratios ($1.0 <$ C/O < 1.05) and then only at the upper end of the expected pressure range ($P > 10$ dyne cm^{-2}), again using solar gas compositions (other than the C/O ratio). The prospects for SiC condensation before graphite worsen if lower metallicities are required (and as discussed above, only AGB stars with lower metallicity are predicted to produce the large heavy Si anomalies like those in SiC 6). Although lower metallicity was not addressed by the above authors, since graphite formation is relatively insensitive to pressure, an order of magnitude reduction in metallicity is analogous to a pressure reduction (Si partial pressure) of the same magnitude. Thus, even at the upper end of the expected pressure range, graphite would be predicted to form before SiC in low-metallicity AGB stars. SiC could still form before graphite at C/O very near unity (e.g., $0.98 <$ C/O $<$ 1; Sharp & Wasserburg 1995), but in such cases graphite would be unlikely to form at all. Although deviations from equilibrium are certainly possible, the equilibrium calculation predictions for AGB outflows as outlined above are in agreement with graphites that contain *s*-process enriched carbides (a marker of AGB origin as argued in Croat et al. 2005). In the ∼50 unique sections of high-density graphites that contained internal (Ti, Zr, Mo)C carbides, in no case was an internal SiC also found (Croat et al. 2005). Thus, both theoretical considerations and observations of AGB graphites suggest that SiC condensation prior to graphite is unlikely to occur in AGB outflows, which buttresses the argument for a massive star origin for SiC-graphite 6. Further, SiC-graphite 5 shows that SiC-graphite grain assemblages do form in massive stars.

In terms of reproducing the isotopic composition of SiC-graphite 6, the SN zones that must contribute material are not significantly different from those for 5 (discussed above), although a smaller contribution from the O-rich zones (∼1%) is necessary. Such mixing exercises predict a C/O ratio slightly above unity and an Si/C ratio of ∼2/3 of the solar value. Under such conditions and at plausible pressures from 10^{-3} to 10^{-5} bars (Lodders & Fegley 1995), SiC formation prior to graphite is not expected. Thus, the disorder evident in the internal SiC may be an indication of its chemical instability in the graphite-forming region, having perhaps formed in a different chemical environment. It could have also been subjected to SN shocks or undergone other weathering prior to encapsulation in the graphite. Observations of more unusual SiCs in graphite are needed to further elucidate their formation conditions.

One intriguing question that remains is why unusual SiCs with large ^{29,30}Si enrichments are disproportionately found within graphites (two of three measured) but far less prevalent in the overall SiC population (in ∼0.01% of population). The *P*, *T* conditions in these regions of massive stars may be such that pressures are lower at the point when the gas cools enough to condense SiC, and thus these lower densities produce

only smaller unusual SiCs (e.g., <500 nm) or perhaps few grains at all. The relative scarcity of unusual SiCs in the overall SiC population could then be explained by differential destruction of smaller SiCs, if not protected by encapsulation in larger graphites. Grain destruction processes in massive stars could disproportionately affect smaller unusual SiCs, and evidence for such differential destruction has been observed in SNe (Dwek et al. 2008; Williams et al. 2006). Further, the disorder observed in SiC 6 may indicate that SiC later becomes chemically unstable, and thus could be preferentially destroyed unless isolated from the gas by encapsulation in graphite. Such destructive processes could explain both the dearth of unusual SiCs in the overall SiC population and their excessive occurrence within graphite. It is possible that unusual SiCs of this type might be more commonly found in the <200 nm size range. The measured SiC population consists predominantly of >1 μm grains, although ~615 KJA (~300 nm; Hoppe et al. 2010), ~1300 KJB SiCs (250–450 nm; Hoppe et al. 2008), and ~1300 Indarch IH6 grains (250–650 nm; Zinner et al. 2007, 2010) have been measured for Si isotopes. Unusual SiC grains Z, H2, and H3 (from Figure 1) with $\delta^{29,30}$Si > +500‰ are all found in smaller size fractions. Thus, along with SiC 5, four of the five grains with the heaviest Si anomalies are found among smaller SiCs, with the only exception being the Amari et al. (1999) unusual SiC from the larger KJG fraction (2–4 μm). Given this clear indication of higher abundance of this type of unusual SiCs among the smaller SiCs, continued Si isotopic measurements among the smallest size fractions are warranted.

As mentioned in the introduction, despite the fact that a significant fraction of the Si produced by massive stars (~40% as calculated from Rauscher et al. 2002 models) is from regions with ^{29,30}Si excesses, such anomalies have not yet been found among over 100 silicates (Bose et al. 2008; Nguyen et al. 2007; Vollmer et al. 2008). This is likely not due to instrumental limitations, as ^{29,30}Si excesses are quite easy to detect even in ~100 nm SiCs within graphite, and many silicates larger than this have undergone Si isotopic measurements. The largest ^{29,30}Si excesses are in SN regions with significant ^{16}O, which should favor the formation of silicates or oxides. The absence of such silicates or oxides may indicate that the massive star regions with ^{29,30}Si enrichments (e.g., O/Ne and O/Si layers) have density versus temperature profiles (e.g., Sedlmayr & Patzer 2004) that are less conducive to refractory grain condensation.

Despite the relative dearth of ^{29,30}Si enrichments among the SiC and silicate grain populations, there are indications that a significant number of unusual SiCs await discovery within graphites. Our results show that ~1% of high-density graphites (6 found among ~750 unique graphites) contain internal SiCs and that these are disproportionately likely to contain ^{29,30}Si excesses. Due to the experimental constraints mentioned earlier, the true SiC-containing fraction is probably slightly higher. Previous SIMS measurements of C and Si isotopic ratios from entire graphite grains are consistent with this estimate. Roughly 3% of graphites lie in the ^{12}C-rich and ^{29,30}Si-rich quadrant (Hynes & Gyngard 2009), although not as extreme in heavy Si enrichment as the unusual SiCs. However, these measurements are consistent with the Si anomalies being carried by internal unusual SiCs, with the large anomalies in SiC diluted by the isotopically more normal Si in graphite. Prior isotopic studies of high-density graphite also show only mild N or other minor element anomalies, even when extreme C anomalies are found (Hoppe et al. 1995; Zinner et al. 1995). Since the nucleosynthetic processes that produce large C anomalies are also expected to alter N isotopic ratios, their absence suggest dilution of such anomalies in high-density graphites by isotopic exchange, either on the meteorite parent body or during processing in the solar system or the laboratory (Zinner et al. 1995). More direct evidence of isotopic dilution in high-density graphites comes from relatively minor N and Si anomalies in graphite 5, which contains an internal SiC with far larger anomalies in these elements (see Table 1). Since both SiC and graphite condensed in nearby environments, it is not unreasonable to assume that they initially had similar isotopic ratios. If true, the isotopic differences between the SiCs and graphites show that isotopic dilution has occurred in high-density graphite, similar to that seen previously in low-density SN graphites (Stadermann et al. 2005). It is not surprising that the SiC phase (e.g., SiC 5) would be less susceptible to isotopic exchange of Si and N, since these anomalous elements are an integral part of the crystal structure (since N may be present as AlN subdomains within SiC), rather than being loosely trapped between layers in the graphite structure. Further, the observed N anomaly dilution within graphite 5 relative to its SiC suggests that the N measurement from graphite 6 (^{14}N/^{15}N = 268 ± 9, normal within errors) does not imply that its internal SiC had solar N ratios. Rather, lacking an N measurement on the internal SiC, we do not have accurate information regarding the original N isotopic composition of SiC-graphite 6. This study and previous isotopic data from entire graphites (that exhibit dilution of minor element anomalies) both suggest that unusual SiCs are significantly more common than would be expected from their abundance in the overall SiC population (~0.01% of population). A significant number of such SiCs were likely hidden within graphites of massive star origin, only to be revealed by correlated TEM and NanoSIMS measurements. Correlated TEM and NanoSIMS studies of large high-density Orgueil graphites with C and Si isotopic anomalies suggestive of the presence of unusual SiCs are planned. The study of larger SiC-containing graphites from the Orgueil meteorite may also make other desirable isotopic data available (e.g., ^{14}N/^{15}N, O ratios, *n*-capture excesses in Ti or other elements), which will help us to further define the unusual SiC subgroup.

6. CONCLUSIONS

Correlated TEM and NanoSIMS investigations have revealed a new type of unusual SiC with large ^{29,30}Si enrichments found inside of graphites from the Murchison meteorite. Although a few such unusual SiCs have been found independent of graphite previously (of ~40,000+ grains measured; Amari et al. 1999; Hoppe et al. 2010; Zinner et al. 2010), two more unusual SiCs (<250 nm in size) were found within graphites, one with Si anomalies as large as $\delta^{29,30}$Si > +1000‰ (more than double the solar ratios). Accompanying ^{12}C enrichments were measured in the SiCs (and a ^{15}N enrichment in one of the SiCs), and while their host graphites had comparable C ratios, the minor element anomalies (Si and N) were not present in the graphites, suggesting dilution via isotopic exchange in the graphite but not the SiC. The magnitude of the heavy Si anomalies in the most anomalous unusual SiC rules out AGB carbon stars (the most prolific producers of carbonaceous stardust), and instead indicates a massive star origin. Such excesses in the heavy Si isotopes can be produced by C-burning and Ne-burning during the post-main-sequence evolution of massive stars (>8 $M_\odot$ initial mass). Since these massive star layers are O-rich, mixing of their heavy Si-enriched material into a C-rich environment is

necessary for condensation of unusual SiC-containing graphites, a process that could occur later in a massive star's evolution, either after mixing in Type II core-collapse SNe or perhaps in the colliding winds of binary W-R stars. The heavy Si anomalies in the second unusual SiC within graphite are lower (δ^{29}Si = +130‰, δ^{29}Si = +290‰), consistent with a massive star origin but also at the upper end of the expected Si isotopic range of low-metallicity AGB stars. However, in this case, a condensation sequence of SiC and then graphite is indicated, and this is not likely to occur in low-metallicity AGB outflows.

Despite their isotopic similarities, TEM analyses of the two unusual SiC-graphites of this study showed diverse microstructures. One unusual SiC was comprised of dozens of separate crystalline domains, similar in appearance to SiC-X grains. Both the 3C and 2H/3C intergrowth polytypes were found among the domains, consistent with those polytypes identified in the overall SiC population. In this case, the SiC was found at the graphite's periphery, suggesting contemporaneous SiC formation with graphite and subsequent entrainment into the graphite during its growth. In the second case, the SiC was found directly at the graphite's center, indicating that SiC condensed first and then acted as a heterogeneous nucleation site for the graphite. This SiC consisted of a single 3C domain but with evidence of disorder, possibly indicating that the SiC had became chemically unstable prior to encapsulation.

That two of the three internal SiCs measured for Si showed large ^{29,30}Si enrichments suggests this isotopic subgroup is less rare than originally estimated, and that such SiCs have been hidden within graphites until discovered by coordinated TEM/NanoSIMS studies. Other SiC-containing graphites found in TEM studies, while too small for Si isotopic measurement, show associated phases or other indications of a massive star origin. Abundance estimates, based on TEM investigations of high-density graphites sliced en-masse and on isotopic measurements of whole graphites, show that unusual SiCs are present in at least ~1% of high-density graphites. The scarcity of grains with ^{29,30}Si isotopic enrichment among the overall SiC population and among silicates suggests P, T conditions less conducive to dust formation and gives indirect evidence for preferential destruction of these smaller unusual SiCs.

We thank Roy Lewis (University of Chicago) and Sachiko Amari (Washington University) for preparing the Murchison KFC1 samples. This material is based on work supported by NASA under grants NNG04GG13G and NNX07AF98G issued through the Office of Space Science.

REFERENCES

Amari, S., Gao, X., Nittler, L., Zinner, E., José, J., Hernanz, M., & Lewis, R. 2001a, ApJ, 551, 1065
Amari, S., Hoppe, P., Zinner, E., & Lewis, R. S. 1992, ApJ, 394, L43
Amari, S., Hoppe, P., Zinner, E., & Lewis, R. S. 1995a, Meteoritics, 30, 679
Amari, S., Lewis, R. S., & Anders, E. 1994, Geochim. Cosmochim. Acta, 58, 459
Amari, S., Nittler, L. R., Zinner, E., Gallino, R., Lugaro, M., & Lewis, R. S. 2001b, ApJ, 546, 248
Amari, S., Nittler, L. R., Zinner, E., Lodders, K., & Lewis, R. S. 2001c, ApJ, 559, 463
Amari, S., Zinner, E., & Lewis, R. S. 1995b, ApJ, 447, L147
Amari, S., Zinner, E., & Lewis, R. S. 1999, ApJ, 517, L59
Arendt, R. G., Dwek, E., & Moseley, S. H. 1999, ApJ, 521, 234
Bernatowicz, T. J., Cowsik, R., Gibbons, P. C., Lodders, K., Fegley, B., Jr., Amari, S., & Lewis, R. S. 1996, ApJ, 472, 760
Bertoldi, F., et al. 2003, A&A, 406, L55
Bose, M., Stadermann, F. J., & Floss, C. 2008, Lunar Planet. Sci., 39, Abstract 1099
Cherchneff, I., Le Teuff, Y. H., Williams, P. M., & Tielens, A. G. G. M. 2000, A&A, 357, 572
Clayton, D. D. 2003, Handbook of the Isotopes: Hydrogen to Gallium (Cambridge: Cambridge Univ. Press)
Clayton, D. D., Deneault, E. A.-N., & Meyer, B. S. 2001, ApJ, 562, 480
Clayton, D. D., & Nittler, L. 2004, ARA&A, 42, 39
Croat, T. K., Bernatowicz, T., Amari, S., Messenger, S., & Stadermann, F. J. 2003, Geochim. Cosmochim. Acta, 67, 4705
Croat, T. K., & Stadermann, F. J. 2006, Lunar Planet. Sci., 37, Abstract 2048
Croat, T. K., & Stadermann, F. J. 2008, Lunar Planet. Sci., 39, Abstract 1739
Croat, T. K., Stadermann, F. J., & Bernatowicz, T. J. 2005, ApJ, 631, 976
Croat, T. K., Stadermann, F., & Bernatowicz, T. 2008, Meteorit. Planet. Sci., 43, 1497
Crowther, P. A. 2007, ARA&A, 45, 177
Daulton, T. L., Bernatowicz, T. J., Lewis, R. S., Messenger, S., Stadermann, F. J., & Amari, S. 2003, Geochim. Cosmochim. Acta, 67, 4743
Douvion, T., Lagage, P. O., & Pantin, E. 2001, A&A, 369, 589
Dwek, E., Galliano, F., & Jones, A. P. 2007, ApJ, 662, 927
Dwek, E., et al. 2008, ApJ, 676, 1029
Ercolano, B., Barlow, M. J., & Sugerman, B. E. K. 2007, MNRAS, 375, 753
Fedkin, A. V., Meyer, B. S., Grossman, L., & Desch, S. J. 2009, Lunar Planet. Sci., 40, Abstract 1699
Fesen, R. A., et al. 2006, ApJ, 636, 859
Gehrz, R. D. 1989, in IAU Symp. 135, Interstellar Dust, ed. L. J. Allamandola & A. G. G. M. Tielens (Dordrecht: Kluwer), 445
Gyngard, F., Nittler, L., Stadermann, F. J., & Zinner, E. 2010, Lunar Planet. Sci., 41, Abstract 1152
Hoppe, P., Amari, S., Zinner, E., & Lewis, R. S. 1995, Geochim. Cosmochim. Acta, 59, 4029
Hoppe, P., Groner, E., Huth, J., & Amari, S. 2010, Lunar Planet. Sci., 41, Abstract 1082
Hoppe, P., Leitner, J., Meyer, B. S., The, L.-S., Lugaro, M., & Amari, S. 2009, ApJ, 691, L20
Hoppe, P., Strebel, R., Eberhardt, P., Amari, S., & Lewis, R. S. 2000, Meteorit. Planet. Sci., 35, 1157
Hoppe, P., Vollmer, C., Heck, P. R., Groener, E., Gallino, R., & Amari, S. 2008, Lunar Planet. Sci., 39, 1025
Hughes, J. P., Rakowski, C. E., Burrows, D. N., & Slane, P. O. 2000, ApJ, 528, L109
Hwang, U., & Laming, J. M. 2003, ApJ, 597, 362
Hynes, K. M., Amari, S., Bernatowicz, T. J., Croat, T. K., & Mertz, A. F. 2008, Lunar Planet. Sci., 39, Abstract 2076
Hynes, K. M., Amari, S., Bernatowicz, T., Croat, T. K., & Mertz, A. 2009, Lunar Planet. Sci., 40, Abstract 1398
Hynes, K. M., Croat, T. K., & Bernatowicz, T. J. 2007, Lunar Planet. Sci., 38, Abstract 1693
Hynes, K. M., & Gyngard, F. 2009, Lunar Planet. Sci., 40, Abstract 1198
Jones, A. P. 2004, in ASP Conf. Ser. 309, Astrophysics of Dust, ed. A. N. Witt, G. C. Clayton, & B. T. Draine (San Francisco, CA: ASP), 347
José, J., Hernanz, M., Amari, S., Lodders, K., & Zinner, E. 2004, ApJ, 612, 414
Lodders, K. 2006, ApJ, 647, L37
Lodders, K., & Fegley, B., Jr. 1995, Meteoritics, 30, 661
Meikle, W. P. S., et al. 2007, ApJ, 665, 608
Messenger, S., Keller, L. P., & Lauretta, D. S. 2005, Science, 309, 737
Meyer, B. S., Weaver, T. A., & Woosley, S. E. 1995, Meteoritics, 30, 325
Nguyen, A. N., Stadermann, F. J., Zinner, E., Stroud, R. M., Alexander, C. M. O. D., & Nittler, L. R. 2007, ApJ, 656, 1223
Nittler, L. R. 1997, in AIP Conf. Proc. 402, Astrophysical Implications of the Laboratory Study of Presolar Materials, ed. T. J. Bernatowicz & E. Zinner (Melville, NY: AIP), 59
Nittler, L. R., & Alexander, C. M. O. D. 2003, Geochim. Cosmochim. Acta, 67, 4961
Nittler, L. R., Alexander, C. M. O. D., Gallino, R., Hoppe, P., Nguyen, A. N., Stadermann, F. J., & Zinner, E. K. 2008, ApJ, 682, 1450
Nittler, L. R., Alexander, C. M. O. D., & Nguyen, A. N. 2006, Meteorit. Planet. Sci., 41, 5316
Nittler, L. R., Alexander, C. M. O. D., Wang, J., & Gao, X. 1998, Nature, 393, 222
Nittler, L. R., & Hoppe, P. 2005, ApJ, 631, L89
Nittler, L. R., et al. 1995, ApJ, 453, L25
Nozawa, T., Kozasa, T., Umeda, H., Maeda, K., & Nomoto, K. I. 2003, ApJ, 598, 785
Prantzos, N., Arnould, M., & Arcoragi, J.-P. 1987, ApJ, 315, 209
Rauscher, T., Heger, A., Hoffman, R. D., & Woosley, S. E. 2002, ApJ, 576, 323

Rho, J., et al. 2008, ApJ, 673, 271
Sedlmayr, E., & Patzer, A. B. C. 2004, in EAS Publ. Ser., The Future Astronuclear Physics, ed. A. Jorissen, et al. (Les Ulis: EDP Sciences), 51
Sharp, C. M., & Wasserburg, G. J. 1995, Geochim. Cosmochim. Acta, 59, 1633
Stadermann, F. J., Croat, T. K., Bernatowicz, T. J., Amari, S., Messenger, S., Walker, R. M., & Zinner, E. 2005, Geochim. Cosmochim. Acta, 69, 177
Stroud, R. M., Nittler, L. R., & Hoppe, P. 2004, Meteorit. Planet. Sci., 39, 5039
Stroud, R. M., O'Grady, M., Nittler, L. R., & O'd, A. C. M. 2002, Lunar Planet. Sci., 33, 1785
Todini, P., & Ferrara, A. 2001, MNRAS, 325, 726
Travaglio, C., Gallino, R., Amari, S., Zinner, E., Woosley, S., & Lewis, R. S. 1999, ApJ, 510, 325
Vollmer, C., Hoppe, P., & Brenker, F. E. 2008, ApJ, 684, 611
Whittet, D. C. B. 1992, Dust in the Galactic Environment (Philadelphia, PA: IOP Publishing)
Williams, B. J., et al. 2006, ApJ, 652, L33
Williams, P. M. 2008, in RevMexAA Conf. Ser. 23, Massive Stars: Fundamental Parameters and Circumstellar Interactions, ed. P. Benaglia, G. L. Bosch, & C. E. Cappa (Mexico City: UNAM), 71
Woosley, S. E., & Weaver, T. A. 1995, ApJS, 101, 181
Yoshida, T. 2007, ApJ, 666, 1048
Zinner, E. 2007, in Treatise on Geochemistry Update (online update only), ed. H. D. Holland, K. K. Turekian, & A. Davis (Oxford: Elsevier Ltd.), 1
Zinner, E., Amari, S., Wopenka, B., & Lewis, R. S. 1995, Meteoritics, 30, 209
Zinner, E., Gyngard, F., & Lin, Y. 2010, Lunar Planet. Sci., 41, Abstract 1359
Zinner, E., Nittler, L. R., Gallino, R., Karakas, A. I., Lugaro, M., Straniero, O., & Lattanzio, J. C. 2006, ApJ, 650, 350
Zinner, E., et al. 2007, Geochim. Cosmochim. Acta, 71, 4786